ACS OMEGA

http://pubs.acs.org/journal/acsodf

Article

Mapping Novel Biomarkers of Liver Injury by Tissue Proteomic Analysis

Bo Yang,* Jianan Zhang, Le Sun, Tingmei Huang, Yaqi Kong, Lei Li, Zhengwang Sun,* Mengchen Yin,* and Xiaotao Li*

Cite This: *ACS Omega* 2021, 6, 7127−7138

Read Online

ACCESS | Metrics & More | Article Recommendations

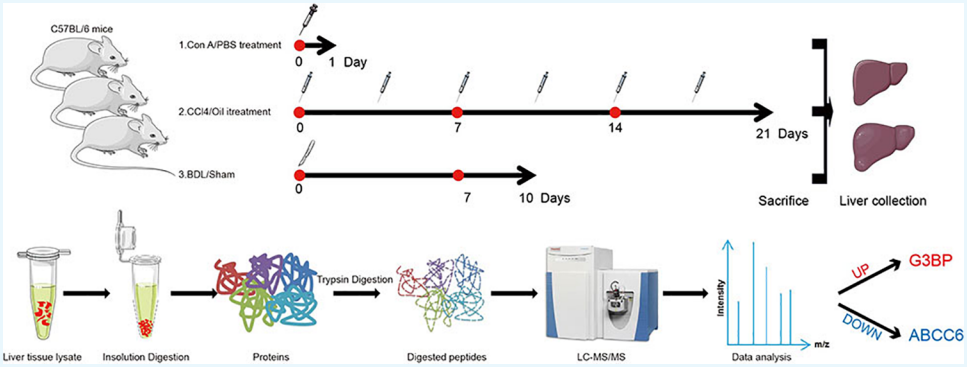

ABSTRACT: Liver damage is a dynamic process, and evaluation of liver injury degree is the key step in disease diagnosis. However, few common markers among different types of liver injury have been reported. Herein, we generated three liver injury mouse models, including Con A-induced, CCl_4-injected, and subjected bile duct ligation mouse models, to simulate different types of liver damage in humans and then performed a label-free mass spectrometry to identify differentially expressed proteins in liver tissues. Interestingly, two proteins, G3BP and ABCC6, were conserved regulated in different liver injury models and are proposed to be biomarkers in liver injury, with G3BP upregulated and ABCC6 downregulated. Overall, our study identified two novel biomarkers of liver injury, and they might be used as potential drug targets of liver damage research studies.

INTRODUCTION

Liver cancer is the fourth leading cause of death worldwide in 2018; meanwhile, liver injuries including liver fibrosis mark the early stage of liver cancer.[1] Therefore, evaluation of the liver injury degree is the key step to understand and timely intervention for patients. More biomarkers for liver fibrosis have been discovered over the past decades and are expected to play a role in clinical practice. However, few common markers among different types of liver injury have been reported, which may help to discover liver injury at an early stage. Mouse models of liver injury,[2] such as chemically induced models, genetically engineered mouse models, and surgery-based models, are used to simulate human liver injury pathology, which helps identify potential biomarkers and develop therapeutic drugs.

Concanavalin A (Con A) is widely used to induce acute hepatic injury in mice through upregulating inflammatory cytokines, for example, IFN-γ[3−5] and tumor necrosis factor-α.[6] Carbon tetrachloride (CCl_4) is a common chemical reagent to induce hepatic fibrosis in mice.[7] It simulates human chronic disease caused by toxic damage in many aspects.[8−10] Common bile duct ligation (BDL), as a surgery-based mouse model, is well known to simulate clinically relevant liver cholestasis model.[8] A doubly ligated bile duct transected between two ligatures causes the obstruction of the bile duct, further increases the biliary pressure and cytokine secretion, and thus generates liver damage.[11,12]

Some biomarkers of liver injury have been reported. G3BP is one of them. G3BP is a secreted glycoprotein which is able to modulate cell adhesion. G3BP is highly expressed in HCV and HCC.[13]

In the present study, we generated three liver injury mouse models, including Con A-induced model, CCl_4-injected model, and subjected BDL mouse model, to simulate different types of liver damage in humans. Then, we identified differentially

Received: January 10, 2021
Accepted: February 22, 2021
Published: March 2, 2021

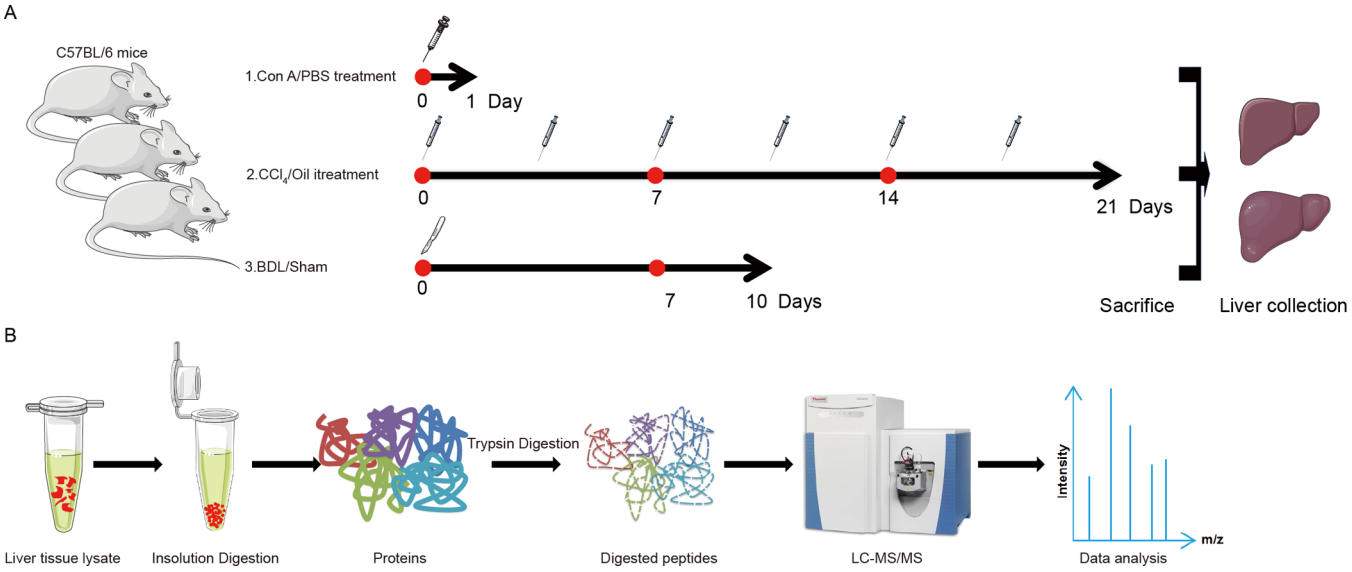

Figure 1. Workflow of the present study. (A) Scheme for the mouse liver injury/hepatic fibrosis model. In this study, mice were bred into C57BL/6, and all the mice were 8−10 weeks old when used in the experiments. Con A (15 mg/kg) injected for 1 day was used to construct the acute liver injury model, and PBS was injected as control. CCl_4 mouse model was standardized, relying on the intraperitoneal administration of CCl_4 at a concentration of 1.6 mg/g body weight two times per week for 3 weeks, and oil was injected as control. The BDL model was subjected to BDL for 10 days, and sham operation served as control. (B) Workflow of quantitative proteomics in this study. Label-free quantitative proteomics was performed on the six groups of mice (three mouse models and each control group) (three mice per each group). Briefly, liver tissues in this study were lysed with RIPA buffer and digested in solution with the enzyme trypsin. The digested peptides were desalted with C18 Stage Tips and analyzed using a Q Exactive HF-orbitrap mass spectrometer which was coupled with a NanoLC-1000 HPLC system. MaxQuant software (Version 1.5.3.30) was used for label-free quantification.

expressed proteins in the liver tissues of the three models through proteomics analysis and further described the biological processes, molecular functions, cellular components, and pathways. The significantly regulated proteins were further compared in the three models to pick out proteins that are both upregulated and downregulated in different models. The mRNA level of the proteins was detected by RT-qPCR. We chose two proteins, namely, G3BP and ABCC6. ABCC6, a protein implicated in Pseudoxanthoma elasticum (PXE), is expressed in several tissues, especially in the liver.[14] Finally, we tested the correlation between the survivorship curve of patients and mouse model proteomics data.

The goal of this study is to find common biomarkers in different liver injuries to provide new insights into understanding the mechanism of liver cancer and exploring new drug targets for liver injury.

RESULTS

Liver Injury Induced in Three Mouse Models. Hepatic fibrosis is commonly associated with chronic hepatitis and chronic liver injury. However, the common biomarkers of acute hepatic injury and liver fibrosis are still lacking. Different mouse models are constructed to discover the mechanism of hepatic fibrosis. A concentration of 15 mg/kg Con A was used to induce an acute liver injury model, and the mice were analyzed after 1 day. The mice were also induced by injecting with 1.6 mg/g CCl_4 two times per week for 3 weeks to stimulate the chemical-induced hepatic fibrosis mouse model. Oil was injected as the control. Besides, BDL for 10 days which induced liver fibrosis/cirrhosis in rodents is well established and widely accepted. Sham operation served as control (Figure 1A). We utilized proteomics analysis based on different hepatic fibrosis mouse models to discover new proteins related to hepatic injury. In short, mouse livers were lysed with RIPA buffer after different treatments and digested to peptides with trypsin for LC−MS/MS analysis based on the label-free quantification method (Figure 1B).

Proteomics Analysis of Con A-Induced Acute Liver Injury Mouse Model. First of all, we detected the pathological changes in a mouse liver after the injection of Con A. Con A-injected mouse liver had a rougher liver surface compared with the noninjected one (Figure 2A). H&E staining showed a much more focal necrosis formation in the injected group (indicated by arrows in Figure 2B). The liver weight to body weight ratio was higher after injection for 1 day (Figure 2C). AST and ALT become elevated whenever disease processes affect the liver cell integrity. We detected ALT and AST activities in the Con A-treated mouse model. Both ALT and AST activities were significantly higher than those of the uninjected ones (Figure 2D,E).

To profile the protein level changes in the Con A-injected mouse model, we performed proteomics analysis based on the label-free quantification method. Totally, 3187 proteins were identified, with 212 upregulated and 205 downregulated (Con A-treated protein intensity to untreated intensity ratio ≥ 1.5, p value ≤ 0.05, as indicated in Figure 2F). The results of Gene Ontology (GO) enrichment analysis are displayed as molecular functions, cellular components, and biological processes (Figure 2G). Most regulated proteins, when injected with Con A, had oxidoreductase activity or transferase activity and were located in extracellular exosomes. Biological process analysis showed that most regulated proteins were associated with the oxidation−reduction process and metabolism, especially lipid metabolism. Kyoto Encyclopedia of Genes and Genomes (KEGG) pathway analysis was performed for proteins with high confidence. The top 10 pathways are shown in Figure 2H, in which the metabolic pathway was the most

https://dx.doi.org/10.1021/acsomega.1c00152
ACS Omega 2021, 6, 7127−7138

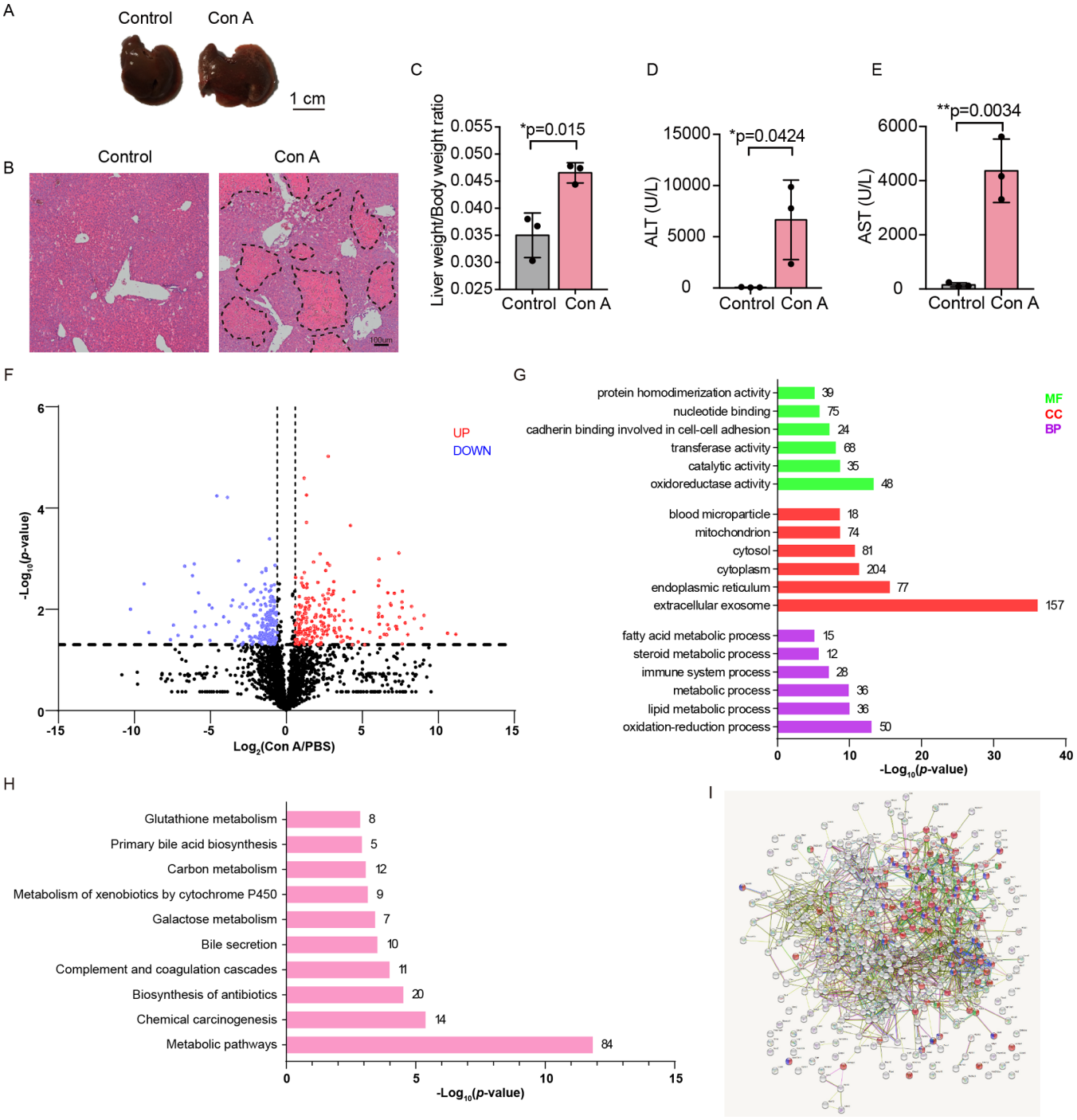

Figure 2. Proteomics analysis of Con A-induced acute liver injury mouse model. (A) Images of the liver surface injected with or without Con A. (B) Liver sections of PBS- or Con A-treated mice were stained with H&E for light microscopy evaluation (×400). Dotted line in (B) indicates focal necrosis. (C) Liver weight to body weight ratios. Quantitative values were obtained by weighing the mice in each group (n: PBS injection = Con A injection = 3). (D,E) Plasma ALT or AST activities of PBS- and Con A-injected mice after 3 weeks of treatment were measured (n: PBS control = Con A = 3). Each value represents mean ± SD (n = 3). *P < 0.05, **P < 0.01; p values were measured by t test. (F) Quantitative proteomics of the Con A-induced mouse liver. The whole proteome of the tissues was analyzed by label-free quantification. Volcano plots of proteins in the Con A-induced group and the PBS-treated control group. The red dots represent proteins that were upregulated at least 1.5 times after Con A treatment (p value < 0.05), and the blue dots represent proteins that were downregulated at least 1.5 times (p value < 0.05) after Con A treatment. (G) GO annotation for molecular function, cell component, and biological process of the different regulated proteins of Con A treatment. The GO terms were enriched by the differentially expressed protein. The significance of the enrichment terms is indicated by the length of the bar. The amount of proteins enriched in each term is shown at the end of the bar chart. (H) Significant top 10 pathways affected by Con A. KEGG pathway analysis was performed for proteins with high confidence, and the number represents proteins enriched in the pathway. The categorization of proteins was done based on molecular functions, cell components, biological processes, and pathways using DAVID (Version 6.8) gene annotation tools. (I) Protein−protein interaction network analysis of proteins during Con A-induced acute liver injury in mice. STRING (Version 11.0) analysis revealed that the proteins for metabolism, metabolism of lipids, and metabolism of amino acids and derivatives of Reactome pathways were found to be associated with each other.

https://dx.doi.org/10.1021/acsomega.1c00152
ACS Omega 2021, 6, 7127−7138

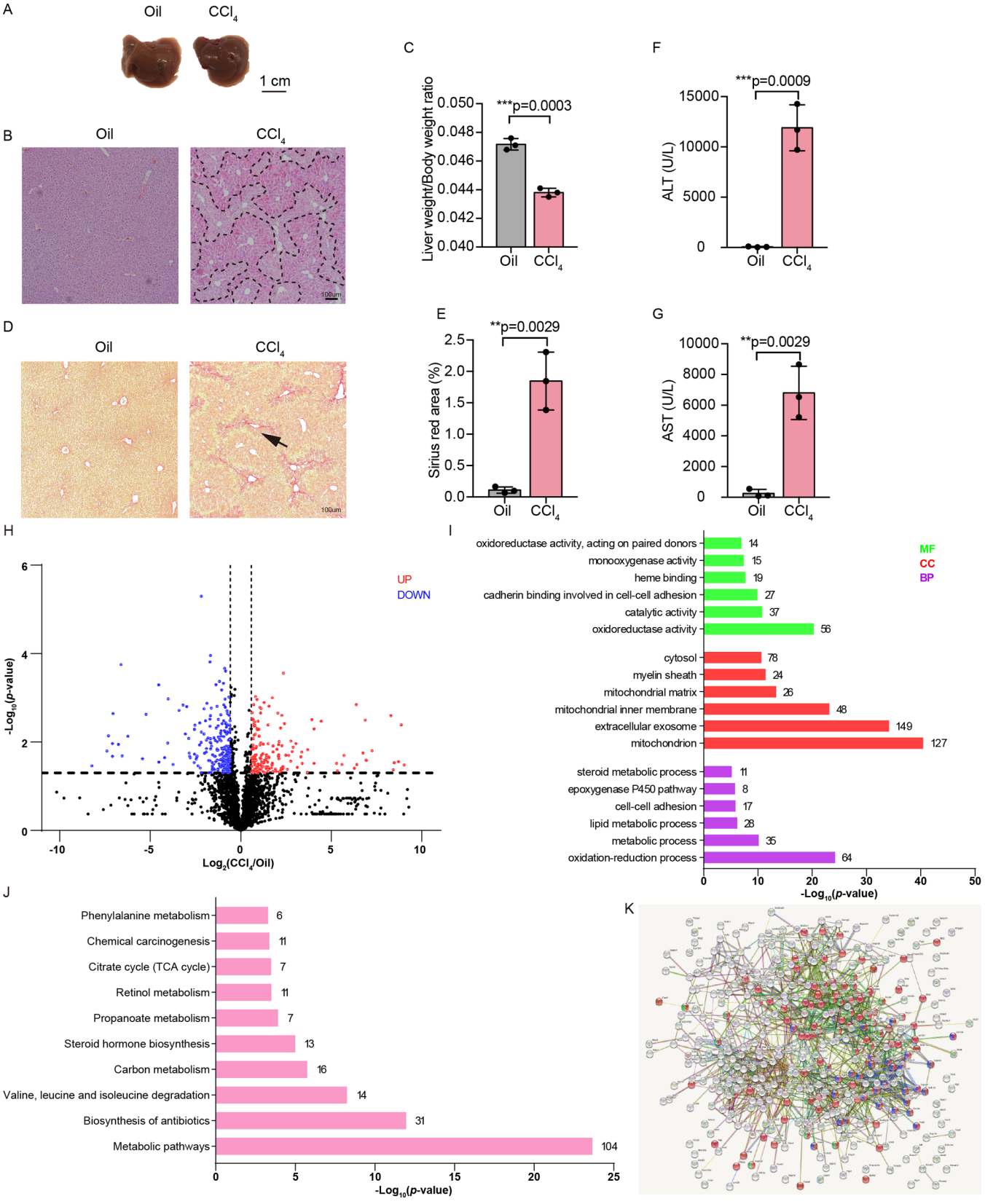

Figure 3. Proteomics analysis of CCl_4-induced liver injury mouse model. (A) Images of the liver surface injected with oil or CCl_4. (B) Liver sections of oil- or CCl_4-injected mice were stained with H&E for light microscopy evaluation (×400). Dotted line in (B) indicates focal necrosis. (C) Liver weight to body weight ratios are shown. Quantitative values were obtained by weighing the mice in each group (*n*: PBS injection = CCl_4 injection = 3). (D,E) Liver sections of oil- or CCl_4-injected mice were stained with Sirius red to identify collagen deposits. The plot shows the Sirius red area over the total area (*n*: oil control = CCl_4 = 3) (×400). Arrows in (D) indicate collagen deposits. (F,G) Plasma ALT or AST activity of oil- or CCl_4-injected mice after 4 weeks treatment was measured (*n*: oil control = CCl_4 = 3). Each value represents mean ± SD (*n* = 3). $*P < 0.05$, $**P < 0.01$, $***P < 0.001$; *p* values were measured by *t* test. (H) Quantitative proteomics of the Con A-induced mouse liver. The whole

https://dx.doi.org/10.1021/acsomega.1c00152
ACS Omega 2021, 6, 7127−7138

Figure 3. continued

proteome of the tissues was analyzed by label-free quantification. Volcano plots of proteins in the CCl_4-induced group and oil-treated control group. The red dots represent proteins that were upregulated at least 1.5 times after CCl_4 treatment (p value <0.05), and the blue dots represent proteins that were downregulated at least 1.5 times (p value < 0.05) after CCl_4 treatment. (I) GO annotation for molecular functions, cell components, and biological processes of the different regulated proteins of the CCl_4 treatment. The GO terms were enriched by the differentially expressed protein. The significance of the enrichment terms is indicated by the length of the bar. The amount of proteins enriched in each term is shown at the end of the bar chart. (J) Significant top 10 pathways affected by CCl_4 are shown. KEGG pathway analysis was performed for proteins with high confidence, and the number represents proteins enriched in the pathway. The categorization of proteins was done based on molecular functions, cell components, biological processes, and pathways using DAVID (Version 6.8) gene annotation tools. (K) Protein−protein interaction network analysis of proteins during CCl_4-induced hepatic fibrosis in mice. STRING (Version 11.0) analysis revealed that the proteins for metabolism, biological oxidation, and metabolism of amino acids and derivatives of Reactome pathways were found to be associated with each other.

notably changed one. We further annotated these proteins with particular functions in one network. Search Tool for the Retrieval of Interacting Genes (STRING) analysis revealed that the proteins for metabolism, lipid metabolism, and amino acid metabolism were related to each other (Figure 2I).

Proteomics Analysis of CCl_4-Induced Liver Injury Mouse Model. Second, the pathological changes in mouse liver after the injection of CCl_4 were analyzed. The liver surface showed the pathological features of liver fibrosis compared with those of the oil-injected mouse (Figure 3A). However, the liver weight to body weight ratio decreased after injection with CCl_4 (Figure 3C). More focal necrosis was found in the injected liver tissue with H&E staining (Figure 3B). Collagen deposits were reflected with Sirius red staining. The degree of liver fibrosis in the injection group was significantly higher than that in the control group, and the collagen deposition was significantly increased (Figure 3E and indicated by arrows in Figure 3D). ALT and AST activities were measured as before. Even higher activities were detected in the CCl_4 group than those in the control group (Figure 3F,G).

We identified 3233 proteins in all using LC−MS/MS, with the intensities of 167 proteins increased and 226 proteins decreased (CCl_4-treated protein intensity to untreated intensity ratio $\geq$ 1.5, p value $\leq$ 0.05, as indicated in Figure 3H). Most of the regulated proteins had oxidoreductase activity or catalytic activity. The majority of them were located in mitochondria and extracellular exosomes (Figure 3I). Most of the proteins participated in the metabolism pathway, with less in the biosynthesis of antibiotics and other pathways (Figure 3J). STRING analysis revealed that the proteins for metabolism, biological oxidation, metabolism of amino acids and derivatives of Reactome pathways were associated with each other (Figure 3K).

Proteomics Analysis of BDL-Induced Cholestatic Liver Injury. Next, we identified regulated proteins in the BDL mouse model. After BDL was performed, the liver surface showed pathological features of cholestatic liver injury in contrast to the sham group, which indicated more focal necrosis (Figure 4A,B). A higher liver weight to body weight ratio was detected in the BDL group (Figure 4C). Much more deposition of collagen is shown in the BDL group (Figure 4D,E). Apart from these, the BDL group showed enhanced ALT and AST activities (Figure 4F,G).

The global proteome profile revealed similar changes in protein levels, as shown before. We identified 3474 proteins totally, of which 428 displayed different expression levels; after BDL, 195 upregulated and 233 downregulated (BDL-treated protein intensity to untreated intensity ratio $\geq$ 1.5, p value $\leq$ 0.05, as indicated in Figure 4H). GO enrichment analysis showed that they mainly localized in the mitochondria and extracellular exosomes with a strong oxidoreductase activity or catalytic activity (Figure 4I). They were enriched in the metabolism pathway and biosynthesis of antibiotics pathway, which correspond with the fact that they were involved in oxidation−reduction, metabolism, and lipid metabolism processes (Figure 4I,J). Proteins for metabolism, lipid metabolism, and biological oxidation were associated with each other based on the STRING analysis (Figure 4K).

Comparison Among Different Liver Injury Mouse Models. To enhance the biomarker amount, we compared the regulated proteins among different liver injury mouse models. We summarized up-, down-, and nonregulated protein numbers (Figure 5A). We overlapped upregulated proteins in the three different experiments and found one common gene. Six common genes were discovered among the downregulated proteins in the three different treatments (Figure 5B). The protein information is listed in Table 1. We performed q-PCR to detect the mRNA level of the six genes in the different liver injury mouse models (all data not shown). Among these, G3BP and ABCC6, which were consistent with the MS data, caught our attention. Protein intensity and the mRNA level of *Lgals3bp* which encodes G3BP in different mouse models were all upregulated, and protein intensity and the mRNA level of *Abcc6* all decreased (Figure 5C,D). Then, we searched a clinical pathological study on G3BP and ABCC6 in liver cancer from the public RNA-seq database (http://kmplot.com). The mean survival time of the patients was calculated by the Kaplan−Meier method (Figure 5E). In 364 patients, the low expression of *Lgals3bp* had a longer survival time. These data corresponded with our finding that *Lgals3bp* upregulated in the liver injury mouse model. In the *Abcc6* survival time graph, we found that the low expression of *Abcc6* had a significantly high hazard ratio in liver cancer, indicating that the expression level of *Abcc6* is negatively correlated with poor progression in liver cancer. These data were also consistent with *Abcc6* downregulated in the liver injury mouse model. However, further study is needed to evaluate the functions of G3BP and ABCC6 in liver injury.

DISCUSSION

Biomarkers of hepatic fibrosis have developed rapidly over the past decades, and some of the biomarkers are subsequently commercial.[15] These biomarkers are useful for patient management and helpful for predicting liver-related morbidity, mortality, and overall survival in clinical trials. However, the causes of liver damage and dynamic changes in liver injury vary, and it is urgent to discover consistent biomarkers of liver diseases.

https://dx.doi.org/10.1021/acsomega.1c00152
ACS Omega 2021, 6, 7127−7138

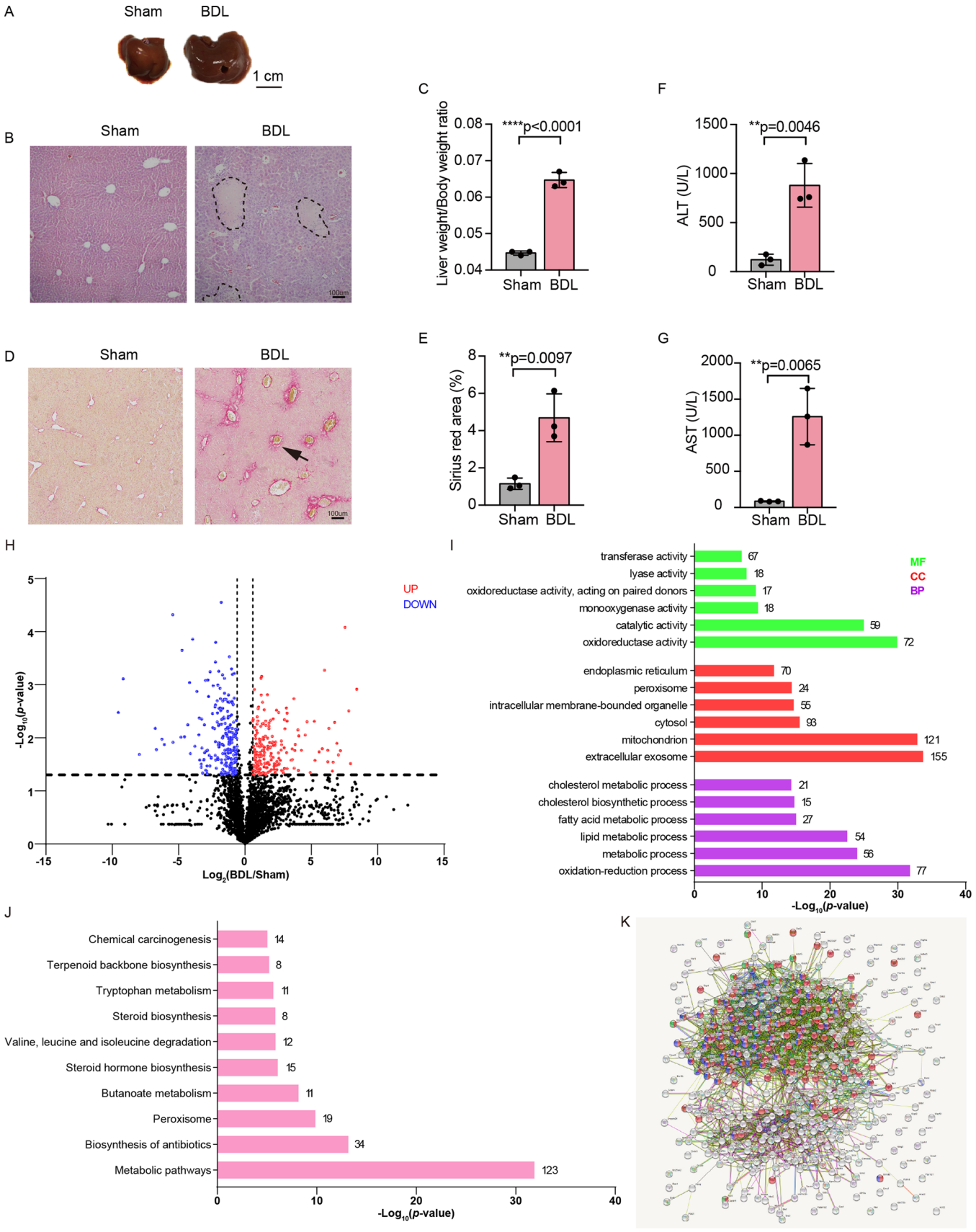

Figure 4. Proteomics analysis of BDL- induced cholestatic liver injury. (A) Images of the liver surface which were subjected to sham or BDL. (B) Liver sections of mice treated with BDL or sham were stained with H&E for light microscopy evaluation (×400). Dotted line in (B) indicates focal necrosis. (C) Liver weight to body weight ratios are shown. Quantitative values were obtained by weighing the mice in each group (*n*: sham control = BDL = 3). (D,E) Liver sections of mice subjected to with sham or BDL were stained with Sirius red to identify the collagen deposits. The plot

https://dx.doi.org/10.1021/acsomega.1c00152
ACS Omega 2021, 6, 7127−7138

Figure 4. continued

shows the Sirius red area over the total area (n: sham control = BDL = 3) (×400). Arrows in (D) indicate the collagen deposits. (F,G) Plasma ALT or AST activity of sham or BDL-treated mice after 4 weeks was measured (n: sham control = BDL = 3). Each value represents mean ± SD (n = 3). $^{**}P < 0.01$, $^{****}P < 0.0001$; p values were measured by t test. (H) Quantitative proteomics of the BDL-induced mouse liver. The whole proteome of the tissues was analyzed by label-free quantification. Volcano plots of proteins in the BDL-subjected group and the sham-treated control group. The red dots represent proteins that were upregulated at least 1.5 times after the BDL treatment (p value <0.05), and the blue dots represent proteins that were downregulated at least 1.5 times (p value < 0.05) after the BDL treatment. (I) GO annotation for molecular functions, cell components, and biological processes of the different regulated proteins of the BDL treatment. The GO terms were enriched by the differentially expressed protein. The significance of the enrichment terms is indicated by the length of the bar. The amount of proteins enriched in each term is shown at the end of the bar chart. (J) Significant top 10 pathways affected by BDL are shown. KEGG pathway analysis was performed for proteins with high confidence, and the number represents proteins enriched in the pathway. The categorization of proteins was done based on molecular functions, cell components, biological processes, and pathways using DAVID (Version 6.8) gene annotation tools. (K) Protein−protein interaction network analysis of proteins during BDL-induced hepatic fibrosis in mice. STRING (Version 11.0) analysis revealed that the proteins for metabolism, metabolism of lipids, and biological oxidation in Reactome pathways were found to be associated with each other.

Proteomic technology is a large-scale study of proteins in tissues and serum.[16−18] There are some novel proteins that have been identified in liver fibrosis by proteomics.[19,20] A follow-up research on the identified proteins can help clinical applications. For example, MFAP4 found with proteomics in liver parenchymal cells has been demonstrated as a biomarker in CHC patients.[25]

In this study, we used three liver injury mouse models to simulate acute hepatic injury and liver fibrosis. First, we detected the pathological changes in mouse liver through tissue staining and liver injury markers in serum. Then, we identified 212 upregulated and 205 downregulated proteins in the Con A treatment group; 167 increased and 226 decreased in CCl_4-induced group, and 195 upregulated and 233 downregulated proteins in the BDL group. We performed GO enrichment and KEGG pathway analysis of these three mouse models, respectively. The summarized functional analysis of these fluctuated proteins showed that the metabolism and oxidation−reduction pathway were most influenced. During annotation, the protein−protein interaction of these regulated proteins by STRING analysis, metabolism, and biological oxidation in Reactome pathways were most impressed. This revealed some identical internal changes in the three different models. These changed proteins may be studied as biomarkers of different models. Next, we found one upregulated protein and six downregulated proteins conserved in three different treatments. We selected one upregulated (G3BP) and one downregulated (ABCC6) protein for mRNA level validation. The results showed that the mRNA level was consistent with the protein level.

G3BP (90K/Mac-2-binding protein, gene named *Lgals3bp*), known as a secreted glycoprotein, is able to promote integrin-mediated cell adhesion.[21] It also plays an important role in immune and cytokine modulation.[22,23] A high expression of G3BP has been reported in various infectious and cancerous diseases, including hepatitis C-related fibrosis.[24] Based on serological and histological detection, it is found that G3BP is a significant biomarker in liver fibrosis and cirrhosis in hepatitis C patients.[19] Ferrín reported that the expression level of G3BP dramatically increased in HCV-infected cirrhotic patients,[13] which was also relevant to HCC development by DIGE analysis. However, there were no significant differences between the tumor groups, with the ELISA test. In our results, the protein and mRNA levels of G3BP increased in the three different mouse models, which is consistent with Cheung's serum proteomics study.[19] In our survival analysis of LGALS3BP data from Kaplan−Meier plotter (liver cancer RNA-seq), there were no significant changes in the different RNA levels. This suggests that G3BP functions distinctively in the different stages of liver injury, but it may play a more significant role in the early stage of injury. ABCC6, also termed as MRP6, is a transmembrane protein that can transport anionic glutathione-conjugated compounds.[25,26] It is highly expressed in the hepatocytes in liver.[27−30] Loss-of-function mutations of ABCC6 reduce the plasma inorganic pyrophosphate (PPi) levels, which cause PXE and type-2 generalized arterial calcification of infancy (GACI).[31−33] Several studies about ABC family reported that ABCC1, ABCC3, and ABCC4 have crucial hepatoprotective effects during BDL.[34,35] Maher suggested that ABCC6 has a minor role in the hepatic transport of bile acids in rats. The ABCC6 mRNA level slightly decreased after 3 days of BDL, but Mrp6 expression was not significantly altered.[14] In this study, we found that ABCC mRNA and protein levels significantly decreased after 10 days of BDL. The different results of the two experiments are probably because of different treatment times. A sharp reduction in protein and mRNA levels was also observed in the other two experiment groups. This indicated the possibility that ABCC6 can be used as a biomarker of liver damage. Survival graphs showed that the higher RNA expression was related to a longer survival time. The consistency between the survival analysis and proteomics, qPCR results, revealed that ABCC6 has an important role in the normal function of liver.

In conclusion, we generated three mouse models and found two protein biomarkers by proteomics technology that can be considered as potentially useful biomarkers for liver injury. G3BP was upregulated and ABCC6 was downregulated in the liver damage models, both in terms of RNA level and protein level. The changes of the two proteins are consistent. However, the mechanism of the two proteins dysregulated in liver injury remains unclear. Further study is needed to reveal their function in liver injury. Because of their sharp changes, G3BP and ABCC6 might be used as potential biomarkers for multiple stages of liver injury.

■ CONCLUSIONS

In conclusion, we generated three mouse models and found two protein biomarkers by proteomics technology that can be considered as potentially useful biomarkers for liver injury. G3BP was upregulated and ABCC6 was downregulated in the liver damage models. Both in terms of RNA level and protein level, the changes of the two proteins are consistent. However, the mechanism of the two proteins dysregulated in liver injury remains unclear. Further study is needed to reveal their function in liver injury. Because of their sharp changes, G3BP

https://dx.doi.org/10.1021/acsomega.1c00152
ACS Omega 2021, 6, 7127−7138

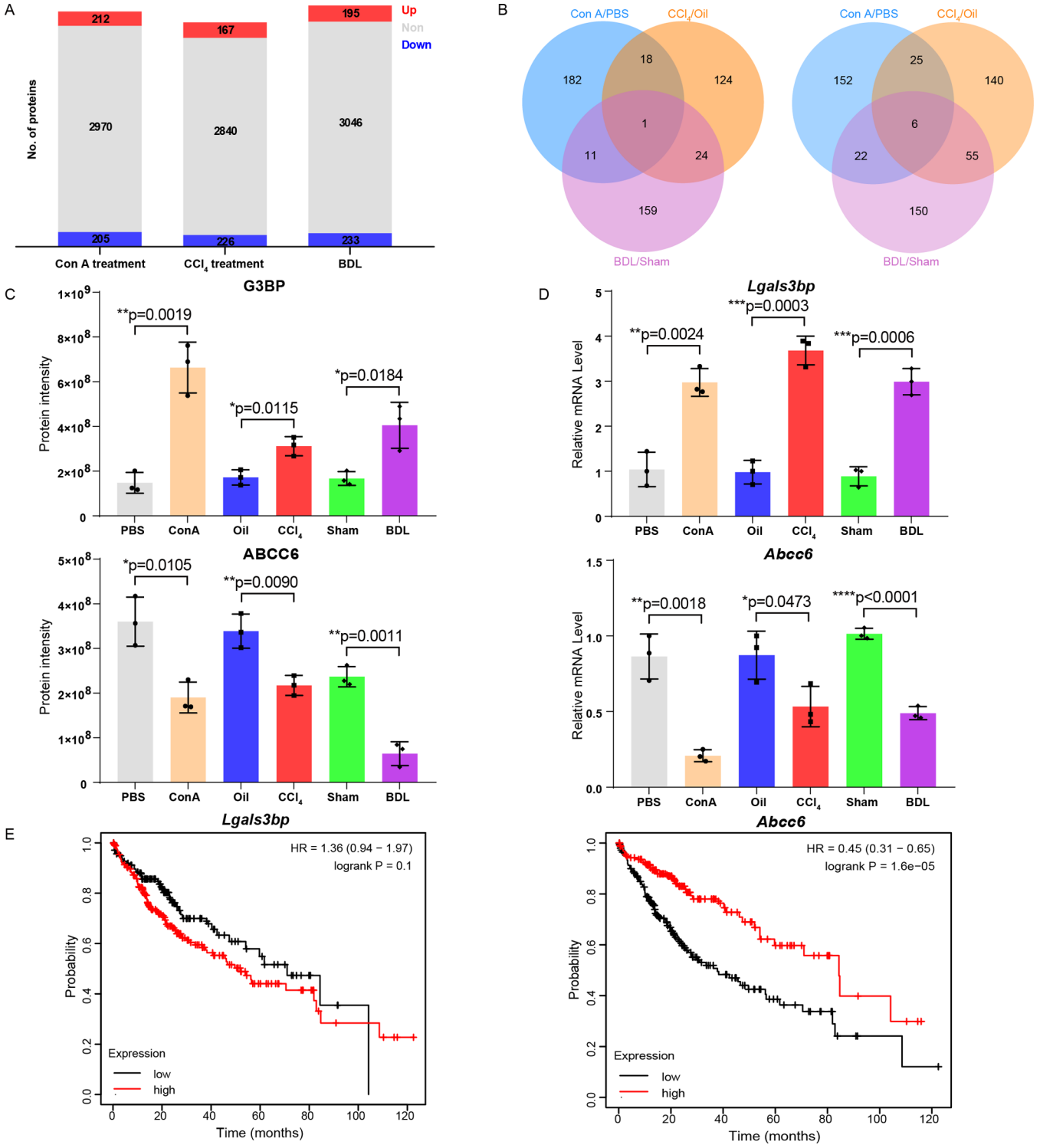

Figure 5. Proteomics comparison of the three different treatments. (A) Numbers of significantly up-, non-, and downregulated proteins among the three different treatments. The red squares represent proteins that were upregulated at least 1.5 times ($p < 0.05$), the gray squares represent proteins that were nonregulated, and the blue squares represent proteins that were downregulated at least 1.5 times ($p < 0.05$). The number in the grid represents the number of cluster proteins. (B) Venn diagrams of upregulated (left panel) and downregulated (right panel) proteins among the three different treatments. Each circle represents the differential proteins among the different treatment groups, and the number in the overlap area represents the number of consistent differentially expressed proteins from multiple comparative groups, and the nonoverlap area represents the unique differentially expressed proteins of each comparative group. (C,D) Protein intensity (C) and relative mRNA level (D) of G3BP (*Lgals3bp*) (upper panel) and Abcc6 (lower panel) are shown. (E) Kaplan−Meier survival functions of *Lgals3bp* (left panel) and *Abcc6* (right panel) are shown. All data were obtained from Kaplan−Meier plotter (http://kmplot.com). The red line represents patients with high protein expression and the black line represents patients with low protein expression. Each value represents mean ± SD ($n = 3$). *$P < 0.05$, **$P < 0.01$, ***$P < 0.001$, ****$P < 0.0001$; p values were measured by t test.

https://dx.doi.org/10.1021/acsomega.1c00152
ACS Omega 2021, 6, 7127−7138

Table 1. Protein List That Coincides with Three Different Treatments[a]

Uniprot ID	Gene name	Treatment	Fold change	p-value	unique peptides	Up/Down
Q07797	Lgals3bp	Con A	2.17	2.09	13	Up
		CCl_4	0.86	1.90	7	
		BDL	1.28	1.33	10	
Q9R0Q6	Arpc1a	Con A	-1.58	1.81	5	Down
		CCl_4	-1.05	1.73	5	
		BDL	-1.33	2.19	6	
Q9JJL3	Slco1b2	Con A	-1.31	1.65	12	Down
		CCl_4	-1.11	2.20	10	
		BDL	-1.15	1.97	10	
Q922D8	Mthfd1	Con A	-1.08	2.16	40	Down
		CCl_4	-0.67	1.38	34	
		BDL	-1.13	1.49	36	
A2AJL3	Fggy	Con A	-1.07	1.52	17	Down
		CCl_4	-0.80	2.34	14	
		BDL	-0.86	1.31	14	
Q9R1S7	Abcc6	Con A	-0.92	1.81	16	Down
		CCl_4	-0.64	1.82	10	
		BDL	-1.88	2.93	13	
Q91X52	Dcxr	Con A	-0.88	1.39	12	Down
		CCl_4	-1.04	2.42	12	
		BDL	-0.66	1.36	10	

[a]Fold change represents the logarithm base 2 value of differentially expressed proteins between the experimental groups and control groups, *p* value represents the negative logarithm base 10 value of differentially expressed proteins between the experimental groups and control groups.

and ABCC6 might be used as potential biomarkers for multiple stages of liver injury.

METHOD DETAILS

Reagents and Materials. Most reagents in this paper were from Sigma-Aldrich (USA) unless otherwise stated. Trypsin was purchased from Promega (USA). TRIzol reagent was obtained from Thermo Fisher Scientific (USA), and reagents for qPCR were purchased from Takara (Japan). All solvents used were of molecular biology or LC−MS grade.

Experimental Animals. Eight to ten weeks old C57BL/6 mice were used for the experiments and bred in-house. All animals were maintained according to the ethical and scientific standards by the Animal Center at East China Normal University (ECNU).

Induction of Liver Injury Model and Treatment Protocol. *Con A-Induced Acute Liver Injury Mouse Model.* Only male mice were injected with ConA in this model. Con A (15 mg/kg) was injected intravenously one time for 1 day to generate an acute hepatic damage model. In control mice, an equal volume of PBS was injected at the same time. In the indicated time point, mice were sacrificed, individual mice blood serums were collected for ALT/AST activity detection, and whole liver tissues were harvested for the analysis of liver injury.

CCl_4 (Carbon Tetrachloride)-Induced Liver Fibrosis Mouse Model. The concentration of CCl_4 was diluted to 40% (0.64 mg/mL) with oil. A C57BL/6 mouse model was injected with CCl_4 at a concentration of 1.6 mg/g body weight two times per week for 3 weeks. An equal volume of oil was injected at the same time. In the indicated time point, mice were sacrificed, and target mice samples were harvested for the analysis of liver fibrogenesis.

BDL-Induced Liver Fibrosis Mouse Model. BDL was performed on mice aged 8−10 weeks for 10 days. To perform BDL, the mice were cut 3 cm in length through a midsection of the abdomen under general anesthesia. The common bile duct was ligated at the adjacent position about 1 cm from the hepatic hilum. The duct is then incised between the two ligation points. At a specified time point, mice were sacrificed, serum and whole liver tissue were collected, and fiber formation was analyzed.

Analysis of Liver Injury and Fibrosis. Liver damage was determined by measuring the ALT/AST activity in plasma. Serum samples were taken from the ocular vein of single mouse at a specified time point after treatment and sent to Adicon Clinical Laboratories (China) for ALT/AST activity detection.

Histological Staining. Paraffin-embedded liver tissues were thinly sliced and stained with H&E in accordance with the standard protocol[36] for light microscopic analysis of liver histology. Briefly, the liver tissues were fixed in 10% neutral-buffered formalin, paraffin-embedded, sectioned at 5 μm thickness, stained with H&E, and evaluated under light microscopy. In some experiments, Sirius red staining was used to detect liver fibrosis.

Sample Preparation and Digestion. Liver tissues from mice were homogenized and lysed by ice-cold RIPA buffer (1% Triton, 0.1% SDS, 50 mM Tris−HCl, pH 7.4, 150 mM NaCl, 2 mM EDTA) with a protease inhibitor cocktail (Roche, Switzerland). The mixture was centrifuged at 20,000*g* for 30 min, and the supernatant protein concentration was determined by BCA assay (Thermo Fisher Scientific, USA).

https://dx.doi.org/10.1021/acsomega.1c00152
ACS Omega 2021, 6, 7127−7138

The same amount of supernatant was precipitated with methanol, chloroform, and water at a ratio of 2.66:1:2. The pellets were dissolved in urea buffer (8 M urea, 100 mM Tris−HCl, pH 8.5). To the solution, 5 mM tris(2-carboxyethyl) phosphine (TCEP) was added to reduce disulfide bridges for 20 min at room temperature. To the solution, 10 mM iodoacetamide was added to alkylate the reduced cysteine residues for 15 min in the dark at room temperature. The urea concentration was diluted to 2 M with Tris buffer (100 mM Tris−HCl, pH 8.5), and 1 mM $CaCl_2$ was added to the solution. The protein mixture was digested by trypsin at 37 °C overnight at a ratio of 1:50 (w/w). The digested peptides were desalted with C18 Stage Tips.

LC−MS/MS and Data Analysis. The peptide mixture was performed on a Q Exactive HF-Orbitrap mass spectrometer, which was coupled with a NanoLC-1000 high-performance liquid chromatography (HPLC) system (Thermo Fisher Scientific, USA). The peptide was directly loaded into a self-made 15 cm capillary column (C18-AQ, 1.9 μm, 100 μm bore). Mobile phase A was composed of 0.1% FA, 2% ACN, and 98% H_2O, whereas the mobile phase B consisted of 0.1% FA, 2% H_2O, and 98% ACN. A gradient of 180 min static flow rate of 300 nL/min (mobile phase B: 3% at 0 min, 8% at 7 min, 20% at 139 min, 30% at 169 min, 95% at 175 min, and 95% at 180 min) was used. The data were obtained in a data-dependent (top 20) mode. The scanning range of MS1 was set to m/z 350−1500 with a resolution of 60,000. The AGC target area was set as 3×10^6, and the maximum injection time was 20 ms. For MS2, the fixed first mass was set to m/z 120. The AGC target area was set at 1×10^5, and the maximum injection time was 45 ms. The precursor peptides were cleaved by high-energy collisional dissociation, and the resulting fragment ions were determined by an Orbitrap analyzer. MS data analysis software MaxQuant (version 1.5.3.30) was used for label-free quantification. The MS data were searched using the SwissProt mouse protein database (downloaded on 26 February, 2018) and the built-in contaminant protein list. The proteins identified in the three replicates were used for quantitative analysis.

Protein Functional Annotation. The UniProt accession ID of the proteome was identified through DAVID Bioinformatics Resources 6.8 for GO annotation and KEGG pathway analysis. Protein−protein interaction network analysis was performed on differentially expressed proteins by using the STRING[37] (version 11.0) database retrieval tool.

Real-Time PCR (qPCR) Analysis. Total RNA was extracted using the TRIzol reagent (Thermo Fisher Scientific, USA) according to the manufacturer's protocol. RNA was transcribed into cDNA using the PrimeScript RT master Mix qPCR (Takara, Japan). Real-time PCR was performed using the TB Green *Premix* Ex TaqII (Takara, Japan). Gene expression levels were calculated based on the $\Delta\Delta Ct$ relative quantification methods. The primers used in this study are as follows:

Lgals3bp (F: 5′-TGCTGGTTCCAGGGACTCAA-3′; R: 5′-CCACCGGCCTCTGTAGAAGA-3′) *Abcc6* (F: 5′-TGCGGCCTATCACTTGCTC-3′; R: 5′-CCAGCAC-CATTTTGGTTTTGAA-3′) and *18S* (F: 5′-GCAAT-TATTCCCCATGAACG-3′; R: 5′-GGCCTCACTAAAC-CATCCAA-3′)

Statistics. Experimental results were presented as mean ± SD. A two-tailed unpaired t test was used for the comparison between two experimental groups. Values of $P \leq 0.05$ were considered statistically significant. GraphPad Prism (Version 8.0.1) was used for statistical calculations.

AUTHOR INFORMATION

Corresponding Authors

Bo Yang − *Shanghai Key Laboratory of Regulatory Biology, Institute of Biomedical Sciences, School of Life Sciences, East China Normal University, Shanghai 200241, China; Interdisciplinary Research Center on Biology and Chemistry, Shanghai Institute of Organic Chemistry, Chinese Academy of Sciences, Shanghai 201210, China;* orcid.org/0000-0002-6068-8826; Email: yangbo6674@163.com

Zhengwang Sun − *Department of Orthopaedic Surgery, Fudan University Shanghai Cancer Center, Shanghai 200032, China*; Email: specialsamsun@126.com

Mengchen Yin − *Department of Orthopaedics, LongHua Hospital, Shanghai University of Traditional Chinese Medicine, Shanghai 201203, China*; Email: yinmengchen0513@126.com

Xiaotao Li − *Shanghai Key Laboratory of Regulatory Biology, Institute of Biomedical Sciences, School of Life Sciences, East China Normal University, Shanghai 200241, China*; Email: xtli@bio.ecnu.edu.cn

Authors

Jianan Zhang − *Interdisciplinary Research Center on Biology and Chemistry, Shanghai Institute of Organic Chemistry, Chinese Academy of Sciences, Shanghai 201210, China; University of Chinese Academy of Sciences, Beijing 100049, China*

Le Sun − *Interdisciplinary Research Center on Biology and Chemistry, Shanghai Institute of Organic Chemistry, Chinese Academy of Sciences, Shanghai 201210, China; University of Chinese Academy of Sciences, Beijing 100049, China*

Tingmei Huang − *Shanghai Key Laboratory of Regulatory Biology, Institute of Biomedical Sciences, School of Life Sciences, East China Normal University, Shanghai 200241, China*

Yaqi Kong − *Shanghai Key Laboratory of Regulatory Biology, Institute of Biomedical Sciences, School of Life Sciences, East China Normal University, Shanghai 200241, China*

Lei Li − *Shanghai Key Laboratory of Regulatory Biology, Institute of Biomedical Sciences, School of Life Sciences, East China Normal University, Shanghai 200241, China;* orcid.org/0000-0001-6990-1825

Complete contact information is available at: https://pubs.acs.org/10.1021/acsomega.1c00152

Author Contributions

B.Y. and J.Z. contributed equally to this work. B.Y., Z.S., M.Y., and X.L. conceived the study and designed the experiments. B.Y. performed most of the experiments. T.H. and Y.K. performed mouse model experiments. J.Z. and L.S. performed mass spectrometry analysis. J.Z., B.Y., and L.L. interpreted the data and wrote the manuscript. All authors read and approved the final manuscript.

Notes

The authors declare no competing financial interest.

The data supporting the results of this study can be obtained from the corresponding authors upon reasonable request.

The mass spectrometry proteomics data have been deposited to the ProteomeXchange Consortium (http://

https://dx.doi.org/10.1021/acsomega.1c00152
ACS Omega 2021, 6, 7127−7138

proteomecentral.proteomexchange.org) via the iProX[38] partner repository with the dataset identifier PXD022716.

■ ACKNOWLEDGMENTS

This work was supported by grants from National Natural Science Foundation of China (82022051, 81401837, 81471066, and 31730017) and the Science and Technology Commission of Shanghai Municipality (20S11901500, 19140900400, 14430712100).

■ REFERENCES

(1) Bray, F.; Ferlay, J.; Soerjomataram, I.; Siegel, R. L.; Torre, L. A.; Jemal, A. Global cancer statistics 2018: GLOBOCAN estimates of incidence and mortality worldwide for 36 cancers in 185 countries. *Ca-Cancer J. Clin.* **2018**, *68*, 394−424.

(2) Yanguas, S. C.; Cogliati, B.; Willebrords, J.; Maes, M.; Colle, I.; van den Bossche, B.; de Oliveira, C. P. M. S.; Andraus, W.; Alves, V. A. F.; Leclercq, I.; Vinken, M. Experimental models of liver fibrosis. *Arch. Toxicol.* **2016**, *90*, 1025−1048.

(3) Ikeda, F.; Shimomura, H.; Miyake, M.; Fujioka, S.-I.; Itoh, M.; Takahashi, A.; Iwasaki, Y.; Sakaguchi, K.; Yamamoto, K.; Higashi, T.; Tsuji, T. Early clearance of circulating hepatitis C virus enhanced by induction therapy with twice-a-day intravenous injection of IFN-beta. *J. Interferon Cytokine Res.* **2000**, *20*, 831−836.

(4) Nomura, H.; Sou, S.; Nagahama, T.; Hayashi, J.; Kashiwagi, S.; Ishibashi, H. Efficacy of early retreatment with interferon beta for relapse in patients with genotype Ib chronic hepatitis C. *Hepatol. Res.* **2004**, *28*, 36−40.

(5) Tanabe, J.; Izawa, A.; Takemi, N.; Miyauchi, Y.; Torii, Y.; Tsuchiyama, H.; Suzuki, T.; Sone, S.; Ando, K. Interferon-beta reduces the mouse liver fibrosis induced by repeated administration of concanavalin A via the direct and indirect effects. *Immunology* **2007**, *122*, 562−570.

(6) Salah, M. M.; Ashour, A. A.; Abdelghany, T. M.; Abdel-Aziz, A.-A. H.; Salama, S. A. Pirfenidone alleviates concanavalin A-induced liver fibrosis in mice. *Life Sci.* **2019**, *239*, 116982.

(7) Aydin, M. M.; Akcali, K. C. Liver fibrosis. *Turk. J. Gastroenterol.* **2018**, *29*, 14−21.

(8) Ding, B.-S.; Cao, Z.; Lis, R.; Nolan, D. J.; Guo, P.; Simons, M.; Penfold, M. E.; Shido, K.; Rabbany, S. Y.; Rafii, S. Divergent angiocrine signals from vascular niche balance liver regeneration and fibrosis. *Nature* **2014**, *505*, 97−102.

(9) Yu, C.; Wang, F.; Jin, C.; Huang, X.; Miller, D. L.; Basilico, C.; McKeehan, W. L. Role of fibroblast growth factor type 1 and 2 in carbon tetrachloride-induced hepatic injury and fibrogenesis. *Am. J. Pathol.* **2003**, *163*, 1653−1662.

(10) Beier, J. I.; McClain, C. J. Mechanisms and cell signaling in alcoholic liver disease. *Biol. Chem.* **2010**, *391*, 1249−1264.

(11) Rodríguez-Garay, E. A.; Agüero, R. M.; Pisani, G.; Trbojevich, R. A.; Farroni, A.; Viglianco, R. A. Rat model of mild stenosis of the common bile duct. *Res. Exp. Med.* **1996**, *196*, 105−116.

(12) Park, K. C.; Park, J. H.; Jeon, J. Y.; Kim, S. Y.; Kim, J. M.; Lim, C. Y.; Lee, T. H.; Kim, H. K.; Lee, H. G.; Kim, S. M.; Kwon, H. J.; Suh, J. S.; Kim, S. W.; Choi, S. H. A new histone deacetylase inhibitor improves liver fibrosis in BDL rats through suppression of hepatic stellate cells. *Br. J. Pharmacol.* **2014**, *171*, 4820−4830.

(13) Ferrín, G.; Ranchal, I.; Llamoza, C.; Rodríguez-Perálvarez, M. L.; Romero-Ruiz, A.; Aguilar-Melero, P.; López-Cillero, P.; Briceño, J.; Muntané, J.; Montero-Álvarez, J. L.; De la Mata, M. Identification of candidate biomarkers for hepatocellular carcinoma in plasma of HCV-infected cirrhotic patients by 2-D DIGE. *Liver Int.* **2014**, *34*, 438−446.

(14) Maher, J. M.; Cherrington, N. J.; Slitt, A. L.; Klaassen, C. D. Tissue distribution and induction of the rat multidrug resistance-associated proteins 5 and 6. *Life Sci.* **2006**, *78*, 2219−2225.

(15) Patel, K.; Benhamou, Y.; Yoshida, E. M.; Kaita, K. D.; Zeuzem, S.; Torbenson, M.; Pulkstenis, E.; Subramanian, G. M.; McHutchison, J. G. An independent and prospective comparison of two commercial fibrosis marker panels (HCV FibroSURE and FIBROSpect II) during albinterferon alfa-2b combination therapy for chronic hepatitis C. *J. Viral Hepatitis* **2009**, *16*, 178−186.

(16) Bell, L. N.; Theodorakis, J. L.; Vuppalanchi, R.; Saxena, R.; Bemis, K. G.; Wang, M.; Chalasani, N. Serum proteomics and biomarker discovery across the spectrum of nonalcoholic fatty liver disease. *Hepatology* **2010**, *51*, 111−120.

(17) Morra, R.; Munteanu, M.; Bedossa, P.; Dargere, D.; Janneau, J.-L.; Paradis, V.; Ratziu, V.; Charlotte, F.; Thibault, V.; Imbert-Bismut, F.; Poynard, T. Diagnostic value of serum protein profiling by SELDI-TOF ProteinChip compared with a biochemical marker, FibroTest, for the diagnosis of advanced fibrosis in patients with chronic hepatitis C. *Aliment. Pharmacol. Ther.* **2007**, *26*, 847−858.

(18) Poon, T. C.; Hui, A. Y.; Chan, H. L.; Ang, I. L.; Chow, S. M.; Wong, N.; Sung, J. J. Prediction of liver fibrosis and cirrhosis in chronic hepatitis B infection by serum proteomic fingerprinting: a pilot study. *Clin. Chem.* **2005**, *51*, 328−335.

(19) Cheung, K. J.; Tilleman, K.; Deforce, D.; Colle, I.; Van Vlierberghe, H. The HCV serum proteome: a search for fibrosis protein markers. *J. Viral Hepatitis* **2009**, *16*, 418−429.

(20) Cheung, K. J.; Tilleman, K.; Deforce, D.; Colle, I.; Van Vlierberghe, H. Proteomics in liver fibrosis is more than meets the eye. *Eur. J. Gastroenterol. Hepatol.* **2008**, *20*, 450−464.

(21) Hellstern, S.; Sasaki, T.; Fauser, C.; Lustig, A.; Timpl, R.; Engel, J. Functional studies on recombinant domains of Mac-2-binding protein. *J. Biol. Chem.* **2002**, *277*, 15690−15696.

(22) Natoli, C.; Iacobelli, S.; Kohn, L. The immune stimulatory protein 90K increases major histocompatibility complex class I expression in a human breast cancer cell line. *Biochem. Biophys. Res. Commun.* **1996**, *225*, 617−620.

(23) Ullrich, A.; Sures, I.; D'Egidio, M.; Jallal, B.; Powell, T. J.; Herbst, R.; Dreps, A.; Azam, M.; Rubinstein, M.; Natoli, C.; Et, A. The secreted tumor-associated antigen 90K is a potent immune stimulator. *J. Biol. Chem.* **1994**, *269*, 18401−18407.

(24) Cheung, K. J.; Libbrecht, L.; Tilleman, K.; Deforce, D.; Colle, I.; Van Vlierberghe, H. Galectin-3-binding protein: a serological and histological assessment in accordance with hepatitis C-related liver fibrosis. *Eur. J. Gastroenterol. Hepatol.* **2010**, *22*, 1066−1073.

(25) Iliás, A.; Urbán, Z.; Seidl, T. L.; Le Saux, O.; Sinkó, E.; Boyd, C. D.; Sarkadi, B.; Váradi, A. Loss of ATP-dependent transport activity in pseudoxanthoma elasticum-associated mutants of human ABCC6 (MRP6). *J. Biol. Chem.* **2002**, *277*, 16860−16867.

(26) Belinsky, M. G.; Chen, Z. S.; Shchaveleva, I.; Zeng, H.; Kruh, G. D. Characterization of the drug resistance and transport properties of multidrug resistance protein 6 (MRP6, ABCC6). *Cancer Res.* **2002**, *62*, 6172−6177.

(27) Kool, M.; van der Linden, M.; de Haas, M.; Baas, F.; Borst, P. Expression of human MRP6, a homologue of the multidrug resistance protein gene MRP1, in tissues and cancer cells. *Cancer Res.* **1999**, *59*, 175−182.

(28) Madon, J.; Hagenbuch, B.; Landmann, L.; Meier, P. J.; Stieger, B. Transport function and hepatocellular localization of mrp6 in rat liver. *Mol. Pharmacol.* **2000**, *57*, 634−641.

(29) Maher, J. M.; Slitt, A. L.; Cherrington, N. J.; Cheng, X.; Klaassen, C. D. Tissue distribution and hepatic and renal ontogeny of the multidrug resistance-associated protein (Mrp) family in mice. *Drug Metab. Dispos.* **2005**, *33*, 947−955.

(30) Scheffer, G. L.; Hu, X.; Pijnenborg, A. C. L. M.; Wijnholds, J.; Bergen, A. A. B.; Scheper, R. J. MRP6 (ABCC6) detection in normal human tissues and tumors. *Lab. Invest.* **2002**, *82*, 515−518.

(31) Bergen, A. A. B.; Plomp, A. S.; Schuurman, E. J.; Terry, S.; Breuning, M.; Dauwerse, H.; Swart, J.; Kool, M.; van Soest, S.; Baas, F.; ten Brink, J. B.; de Jong, P. T. V. M. Mutations in ABCC6 cause pseudoxanthoma elasticum. *Nat. Genet.* **2000**, *25*, 228−231.

(32) Le Saux, O.; Urban, Z.; Tschuch, C.; Csiszar, K.; Bacchelli, B.; Quaglino, D.; Pasquali-Ronchetti, I.; Pope, F. M.; Richards, A.; Terry, S.; Bercovitch, L.; de Paepe, A.; Boyd, C. D. Mutations in a gene encoding an ABC transporter cause pseudoxanthoma elasticum. *Nat. Genet.* **2000**, *25*, 223−227.

https://dx.doi.org/10.1021/acsomega.1c00152
ACS Omega 2021, 6, 7127−7138

(33) Ringpfeil, F.; Lebwohl, M. G.; Christiano, A. M.; Uitto, J. Pseudoxanthoma elasticum: mutations in the MRP6 gene encoding a transmembrane ATP-binding cassette (ABC) transporter. *Proc. Natl. Acad. Sci. U.S.A.* **2000**, *97*, 6001−6006.
(34) Pei, Q.; Kobayashi, Y.; Tanaka, Y.; Taguchi, Y.; Higuchi, K.; Kaito, M.; Ma, N.; Semba, R.; Kamisako, T.; Adachi, Y. Increased expression of multidrug resistance-associated protein 1 (mrp1) in hepatocyte basolateral membrane and renal tubular epithelia after bile duct ligation in rats. *Hepatol. Res.* **2002**, *22*, 58−64.
(35) Wagner, M.; Fickert, P.; Zollner, G.; Fuchsbichler, A.; Silbert, D.; Tsybrovskyy, O.; Zatloukal, K.; Guo, G. L.; Schuetz, J. D.; Gonzalez, F. J.; Marschall, H.-U.; Denk, H.; Trauner, M. Role of farnesoid X receptor in determining hepatic ABC transporter expression and liver injury in bile duct-ligated mice. *Gastroenterology* **2003**, *125*, 825−838.
(36) Lefkowitch, J. H. Special stains in diagnostic liver pathology. *Semin. Diagn. Pathol.* **2006**, *23*, 190−198.
(37) Szklarczyk, D.; Morris, J. H.; Cook, H.; Kuhn, M.; Wyder, S.; Simonovic, M.; Santos, A.; Doncheva, N. T.; Roth, A.; Bork, P.; Jensen, L. J.; von Mering, C. The STRING database in 2017: quality-controlled protein-protein association networks, made broadly accessible. *Nucleic Acids Res.* **2017**, *45*, D362−D368.
(38) Ma, J.; Chen, T.; Wu, S.; Yang, C.; Bai, M.; Shu, K.; Li, K.; Zhang, G.; Jin, Z.; He, F.; Hermjakob, H.; Zhu, Y. iProX: an integrated proteome resource. *Nucleic Acids Res.* **2019**, *47*, D1211−D1217.

https://dx.doi.org/10.1021/acsomega.1c00152
ACS Omega 2021, 6, 7127−7138